Existence and dynamics of solitary waves in a two-dimensional Noguchi nonlinear electrical network

Guy Roger Deffo,[1,*] Serge Bruno Yamgoué,[2,†] and François Beceau Pelap[1,‡]

[1]*Unité de Recherche de Mécanique et de Modélisation des Systèmes Physiques (UR-2MSP), Département de Physique, Université de Dschang, BP 69 Dschang, Cameroon*

[2]*Department of Physics, Higher Teachers Training College Bambili, The University of Bamenda, PO. Box 39 Bamenda, Cameroon*

(Received 10 August 2018; published 3 December 2018)

In this work, we investigate solitary waves in a nonlinear two-dimensional discrete electrical lattice. It is made of several of the well-known Noguchi electrical transmission lines, that are transversely or longitudinally coupled to one another by an inductor L_2 or L_1 and a capacitor C_2 or C_1 mounted in parallel. The linear dispersion law of the network is given and the effects of the transverse coupling elements L_2 and C_2 on the allowed bandwidth frequencies are examined. Using the continuum limit approximation, we show that the dynamics of the small amplitude signals in the network can be governed by a (2+1)-dimensional generalized modified Zakharov-Kuznetsov equation. The fixed points of our model equation are examined and the bifurcations of its phase portrait are presented, as functions of the wave velocity of the signals that are to propagate in lattice. Likewise, we derive exact explicit solutions that are possible under different wave velocities and for physically realistic values of the network's parameters. These include pulse, kink, and anti-kink wave solutions and correspond to some special level curves of the first integral of the model equation. We find out that the transverse coupling parameters considerably affect the characteristics of the waves that are propagated throughout the system. Direct numerical simulations are also performed on the exact equations of the network and the results are in agreement with the analytical predictions.

DOI: 10.1103/PhysRevE.98.062201

I. INTRODUCTION

The investigation of wave propagation in dispersive discrete nonlinear media is nowadays well established as an important research field. The great deal of attention devoted to such media was arguably triggered by both the so-called recurrence phenomenon observed originally in the dynamics of one such medium by Fermi-Pasta-Ulam [1], and the concept of soliton that Zabusky-Kruskal used to explain this phenomenon [2]. Since then, research efforts have revealed that dispersive discrete nonlinear media bear many interesting features whose applications extend to different aspects of life, nonlinear optics, plasma physics, biophysics [3–9].

The nonlinear electrical transmission lines (NLTLs) are typical examples of these dispersive nonlinear media. They are convenient tools to study wave propagation in nonlinear dispersive media. In particular, they provide a useful way to check how the nonlinear excitations behave inside the nonlinear medium and to model the exotic properties of new systems [10]. For instance, the propagation of the first-order Korteweg–de Vries (KdV) solitons have been investigated experimentally through the Noguchi model of NLTL [11]. This network was also exploited to carry out theoretical and experimentally investigations of the motion of the second-order KdV solitons using the Toda potential [12,13]. Pelap *et al.* studied the dynamics of peak soliton and bubble soliton waves in a one-dimensional (1D) dispersive nonlinear electrical lattice [14]. This author and other coworkers investigated the dynamics and properties of waves in a modified Noguchi electrical transmission line [15]. Recently, Kengne *et al.* showed that the dynamics of matter-wave solitons in a nonlinear LC transmission network can be modeled by a 1D Gross-Pitaevskii equation with both a chemical and a time-dependent linear potentials [16]. More recently, these authors have also investigated the effects of both the second-neighbor coupling and the strength of the linear potential on the dynamics of modulated waves along a modified Noguchi nonlinear electrical network [17]. Other examples of this nature abound in the study of nonlinear discrete electrical transmission lines where various arrangements of the basic electrical components (resistors, inductors, capacitors) are realized [18–23].

The above cited studies have achieved very interesting and encouraging results. However, they largely consider single NLTL, which limits the applicability of those results to only one-dimensional phenomena. Yet, there are many physical phenomena which cannot be properly understood within the one-dimensional framework. For example, the single NLTL gives a good description of the classic Fermi-Pasta-Ulam (FPU) system [1] while it fails for description of two-dimensional (2D) FPU lattice [24]. Similarly, the single NLTL cannot describe wave propagation in isothermal multicomponent magnetized plasma [25]. In addition, various works have investigated the dynamics of nonlinear excitations in two- and three-dimensional atomic lattices [26,27], but investigations that deal with their electrical counterparts are comparatively scarce [22,28]. The few works reported on 2D electrical

*guyrdeffo@yahoo.fr
†sergebruno@yahoo.fr
‡fbpelap@yahoo.fr,francois.pelap@univ-dschang.org

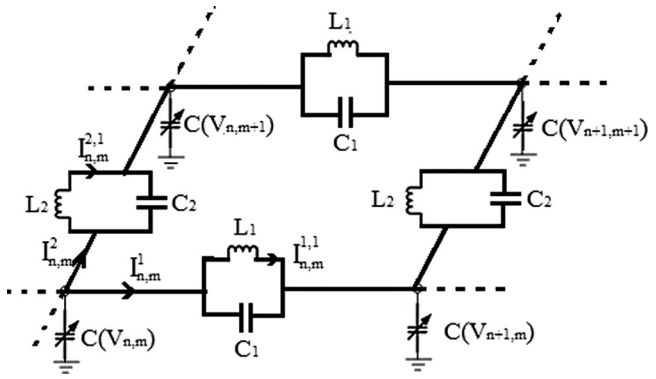

FIG. 1. Part of the system of the two-dimensional nonlinear transmission network. Each cell contains the nonlinear capacitor $C(V)$ in the shunt branch which induces the standard nonlinearity, while in the series propagation and transverse branches, we have the linear inductors L_1 and L_2, and the linear capacitors C_1 and C_1.

lattices include an experimental study of discrete solitons [29], the investigation of the modulational instability phenomenon and the stability of transverse solitary waves [30–32], the recent prediction and analysis of rogue wave using the nonlinear Schrodinger equation [33], and the analytical determination of the expressions of the waves that can propagate in such media [34–42].

In this paper, we aim to broaden the understanding of 2D electrical lattices as propagating media. Specifically, we undertake herein the investigation of the dynamics of transverse solitary waves in a two-dimensional nonlinear electrical transmission line which is presented along with its exact dynamical equation in the next section. In Sec. III, we first show that small amplitude signals in the network can be governed by a generalized modified Zakharov-Kuznetsov equation. Next the dynamics of this equation is studied. In Sec. IV, we investigate the exact soliton solutions of the governing equation and their profiles are portrayed. Numerical investigations are performed in Sec. V in order to verify the validity of the theoretical prediction. We conclude our paper in Sec. VI.

II. MODEL DESCRIPTION AND DYNAMIC EQUATION

The model under consideration is a spatially periodic electrical network whose elementary section, represented in Fig. 1, is a two-dimensional rectangular loop. The nodes of this loop are labeled with two discrete coordinates n and m in the mutually perpendicular directions of the plane. In either direction, there exists a linear inductor and a linear capacitor that are connected in parallel in-between two consecutive nodes. These linear electrical components are taken to be identical along each direction but are assumed to be different from one to the other direction. That is, the coupling inductor and capacitor are $\{L_1, C_1\}$ in the n direction but are $\{L_2, C_2\}$ in the m direction. Through this specific configuration the whole network can always be viewed as transversely coupled Noguchi electrical transmission lines independently of which of these directions is chosen as longitudinal. For definiteness, we shall refer to the n direction as the longitudinal and so, the m direction shall be the transverse direction. The nonlinearity is introduced in the network by a varicap diode which admits that the capacitance varies with the applied voltage. The voltage $V_{n,m}$ and the nonlinear electrical charge $Q_{n,m}$ at the (n, m)th node are related by the polynomial form [15–17,43–45]

$$Q_{n,m} = C_0\left(V_{n,m} - \alpha V_{n,m}^2 + \beta V_{n,m}^3\right), \tag{1}$$

where C_0 is the characteristic capacitance, β and α are nonlinear positive constants.

By applying Kirchhoff laws to the circuit loop of Fig. 1, we obtain the following equations: $L_1\frac{dI^1_{n,m}}{dt} = V_{n,m} - V_{n+1,m}$, $L_2\frac{dI^2_{n,m}}{dt} = V_{n,m} - V_{n,m+1}$, $I^1_{n,m} - I^{1,1}_{n,m} = C_1\frac{d}{dt}(V_{n-1,m} - V_{n,m})$, $I^2_{n,m} - I^{2,1}_{n,m} = C_2\frac{d}{dt}(V_{n,m-1} - V_{n,m})$, and $\frac{dQ_{n,m}}{dt} = I^1_{n-1,m} - I^1_{n,m} + I^2_{n,m-1} - I^2_{n,m}$. The differential equations governing dynamics of voltage signals in the network can then be obtained from the latter using some straightforward algebraic manipulations. They read

$$\begin{aligned}
&\frac{d^2V_{n,m}}{dt^2} - \alpha\frac{d^2V^2_{n,m}}{dt^2} + \beta\frac{d^2V^3_{n,m}}{dt^2}\\
&= u_{01}^2(V_{n+1,m} + V_{n-1,m} - 2V_{n,m})\\
&\quad + u_{02}^2(V_{n,m+1} + V_{n,m-1} - 2V_{n,m})\\
&\quad + C_{r1}\frac{d^2}{dt^2}(V_{n-1,m} + V_{n+1,m} - 2V_{n,m})\\
&\quad + C_{r2}\frac{d^2}{dt^2}(V_{n,m-1} + V_{n,m+1} - 2V_{n,m})
\end{aligned} \tag{2}$$

with $n = 1, 2, \ldots, N$, $m = 1, 2, \ldots, M$, $u_{01}^2 = 1/L_1C_0$, $u_{02}^2 = 1/L_2C_0$, $C_{r1} = C_1/C_0$, and $C_{r2} = C_2/C_0$. N and M correspond to the number of cells considered in the n and m directions, respectively.

The corresponding linear dispersion law describing small amplitude waves of the form $A_0\exp(i(k_1n + k_2m - \omega t))$ is given by

$$\omega^2 = \frac{4u_{01}^2\sin^2\left(\frac{k_1}{2}\right) + 4u_{02}^2\sin^2\left(\frac{k_2}{2}\right)}{1 + 4C_{r1}\sin^2\left(\frac{k_1}{2}\right) + 4C_{r2}\sin^2\left(\frac{k_2}{2}\right)}. \tag{3}$$

For values of k_i chosen in the Brillouin zone $(0 < k_i < \pi)$ with $i = 1, 2$, Fig. 2 represents the evolution of the angular frequency for the n directions and for two specific values of transversal wave numbers k_2. Figure 2(a) obtained for $k_2 = 0$ shows that the system behaves evidently like a pass-lower filter with the cutoff frequency $f_{c1} = \omega(\pi, 0)/2\pi = \sqrt{(4u_{01}^2)/(1 + 4C_{r1})}/2\pi$. This cutoff frequency f_{c1} decreases with the growth of C_{r1}, which means that the linear dispersive component C_1 contributes to reduce the network effects on the wave during its motion. When $k_2 = \pi$, the system behaves like a pass-band filter with lower cutoff frequency and upper cutoff frequency given by $f_{c2} = \omega(0, \pi)/2\pi = \sqrt{(4u_{02}^2)/(1 + 4C_{r2})}/2\pi$ and $f_{c3} = \omega(\pi, \pi)/2\pi = \sqrt{(4u_{01}^2 + 4u_{02}^2)/(1 + 4C_{r1} + 4C_{r2})}/2\pi$, respectively, as can be seen on Fig. 2(b).

The terms proportional to u_{02} and C_{r2} in the right-hand side of Eq. (3) are the transverse direction's contribution to the angular frequency. For a given value of one, we can determine the effect of the other. For example, when C_{r2} vanishes, that

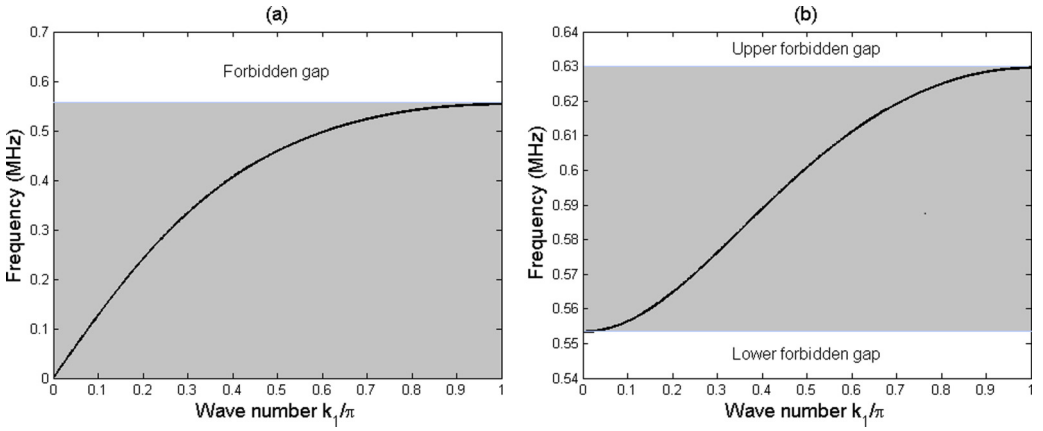

FIG. 2. The linear dispersion curve of the network according of the wave vector k_1(rad/cell) for $u_{01} = 2.5786 \times 10^6$ rad/s and $C_{r1} = 0.3$: (a) $k_2 = 0$, $u_{02} = u_{01}$, $C_{r2} = C_{r1}$. (b) $k_2 = \pi$, $u_{02} = u_{01}$, $C_{r2} = C_{r1}$.

is $C_2 = 0$, the linear dispersion relation (3) becomes

$$\omega^2 = \frac{4u_{01}^2 \sin^2\left(\frac{k_1}{2}\right)}{1 + 4C_{r1}\sin^2\left(\frac{k_1}{2}\right)} + \frac{4u_{02}^2 \sin^2\left(\frac{k_2}{2}\right)}{1 + 4C_{r1}\sin^2\left(\frac{k_1}{2}\right)}. \qquad (4)$$

It is clearly seen that the second term in the right-hand side of the above relation is the inductive coupling contribution to the angular frequency. We remark that the inductive coupling can increase the bandwidth of allowed frequencies as shown in Fig. 3(a) in which there is a large difference between the different considered values of inductive coupling. We can also note that the upper gap zone increases with L_2. Therefore, the model is also appropriate for the investigation of upper gap soliton dynamics. Likewise, for given value of the inductive coupling, the effect of the capacitive coupling can be observed. Figure 3(b) shows the dispersion graph for various values of capacitive coupling C_2. It is also seen that the bandwidth of allowed frequencies increases with parameter C_2. On the other hand, The cutoff frequencies f_{c2} and f_{c3} decrease with the growth of C_2, which means that the linear dispersive component C_2 contributes to reduce the network effects on the wave during its motion.

From the above results, we can use the capacitive and inductive coupling to increase the number of frequencies that the network can support, and this allows transmission of several pieces of information in the network. Also, an increase in the coupling parameters C_2 and L_2 results in a removal of some frequency domain. Therefore, an appropriate choice of these parameters can enable the passage of a low frequency mode or a high frequency mode as presented on Fig. 3. This makes our model of NLTL very interesting. In fact, one can observe that it is very general and encompasses numerous bi-dimensional NLTL considered in the literature. For instance, in the limit case where $L_2 \to \infty$, one recovers the model studied by Kengne *et al.* [31,32]. Similarly, it reduces to the NLTL model investigated in [33,35–37,39–42] if one sets $C_1 = 0$ and $L_2 \to \infty$. It can also reduce to the discrete network model for which Tala-Tebue *et al.* derived envelope periodic waves using the Jacobi elliptic functions [30,38]. Next, this model has the same configuration in both the longitudinal and transverse directions, that is, L_1C_1 and L_2C_2, respectively. Hence, each direction can be considered as the dominant direction of motion. In other words, the presence of the linear inductor L_2 in transverse direction induces a possible transversal wave speed which could not

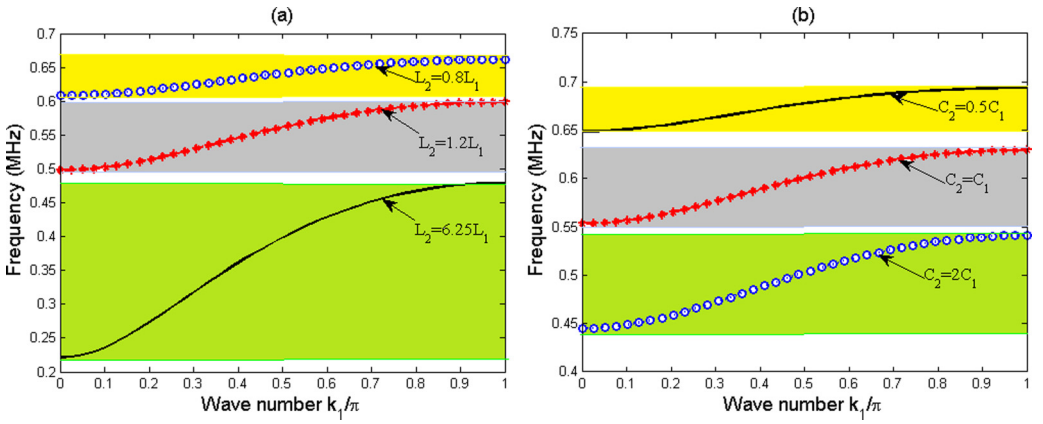

FIG. 3. Effect of the coupling element on the linear dispersion curve of the network showing evolution of the frequency $f = \omega/2\pi$ as a function of the wave number k_1(rad/cell) for $C_0 = 320pF$, $C_1 = 96pF$, $L_1 = 470\mu H$ and $k_2 = \pi$: (a) $C_2 = C_1$, $L_2 = 0.8L_1$, $1.2L_1$, and $6.25L_1$. (b) $L_2 = L_1$, $C_2 = 0.5C_1$, C_1, and $2C_1$.

exist in the previous studies. Finally, as we will see below, this model gives us the possibility to control the shape and the speed of solitary wave using the coupling elements.

III. GENERALIZED MODIFIED ZAKHAROV-KUZNETSOV EQUATION AND DYNAMICAL STUDIES

A. Generalized modified Zakharov-Kuznetsov equation

Now, we turn our attention to the characteristic ordinary differential (ODE) equation of the network which is modeled by Eq. (2). The developments presented below in this view are effected within the continuum medium approximation. That is, we assume that the excited wavelengths, say λ, are much longer than the cell sizes. Denoting the latter by s_1 in the longitudinal direction and s_2 in the transverse direction, we introduce the dimensionless continuous variables $n' = ns_1/\lambda$ and $m' = ms_2/\lambda$ and let $V_{n,m}(t) \longrightarrow V(n', m', t)$. Then, quantities of the form $V_{n\pm\tilde{n},m\pm\tilde{m}}(t)$ for $\tilde{n}, \tilde{m} \in \{-1, 1\}$ become $V(n' \pm s_1/\lambda, m' \pm s_2/\lambda)$ and may be expanded in power series of $1/\lambda$ since $s_1, s_2 \ll \lambda$. Neglecting terms higher than $(1/\lambda)^3$ and defining

$$\overline{u}_{01} = u_{01}\frac{s_1}{\lambda}, \quad \overline{C}_{r1} = C_{r1}\left(\frac{s_1}{\lambda}\right)^2,$$
$$\overline{u}_{02} = u_{02}\frac{s_2}{\lambda}, \quad \overline{C}_{r2} = C_{r2}\left(\frac{s_2}{\lambda}\right)^2, \tag{5}$$

we obtain from Eq. (2) the following two-dimensional partial differential equation (PDE) for the perturbed voltage V:

$$\frac{\partial^2}{\partial t^2}(V - \alpha V^2 + \beta V^3) - \overline{u}_{01}^2\frac{\partial^2 V}{\partial n'^2} - \overline{u}_{02}^2\frac{\partial^2 V}{\partial m'^2} - \overline{C}_{r1}\frac{\partial^2}{\partial t^2}\left(\frac{\partial^2 V}{\partial n'^2}\right) - \overline{C}_{r2}\frac{\partial^2}{\partial t^2}\left(\frac{\partial^2 V}{\partial m'^2}\right) = 0. \tag{6}$$

It is interesting to notice here from Eq. (5) that if $s_1 = s_2 = s$ as we assume onward, then the effects of the cell sizes relative to the wavelength s/λ is, to the current order of truncation, exactly the same as replacing the characteristic capacitance C_0 in Eq. (1) by $C_0' = C_0\lambda/s$.

To find the solitary wave solutions of this equation we introduce the Gardner-Morikawa transformation of the independent variables. This specific transformation is widely used for the analytical investigation of nonlinear discrete lattices [23,34,39,46] owing to its feature of properly balancing the nonlinearity and dispersion after expansion. For our two-dimensional network, it reads as [34]

$$V = \epsilon\psi(x, y, \tau), \quad x = \epsilon^{\frac{1}{2}}(n' - \upsilon_1 t),$$
$$y = \epsilon^{\frac{1}{2}}(m' - \upsilon_2 t), \quad \tau = \epsilon^{\frac{3}{2}}t, \tag{7}$$

where $\epsilon \ll 1$ is a formal parameter. The first of these equations expresses the smallness of the perturbation voltage as compared with the equilibrium value, which may also be necessary for the continuity assumption to be valid. The use of these variables also implies that the time and space derivative operators are transformed according to

$$\frac{\partial}{\partial t} = \epsilon^{\frac{3}{2}}\frac{\partial}{\partial \tau} - \epsilon^{\frac{1}{2}}\upsilon_1\frac{\partial}{\partial x} - \epsilon^{\frac{1}{2}}\upsilon_2\frac{\partial}{\partial y}, \tag{8}$$

$$\frac{\partial^2}{\partial^2} = \epsilon\left(\upsilon_1\frac{\partial}{\partial x} + \upsilon_2\frac{\partial}{\partial y}\right)^2 + \epsilon^3\frac{\partial^2}{\partial \tau^2} - \epsilon^2\left[2\left(\upsilon_1\frac{\partial}{\partial x} + \upsilon_2\frac{\partial}{\partial y}\right)\frac{\partial}{\partial \tau}\right], \tag{9}$$

$$\frac{\partial^2}{\partial n'^2} = \epsilon\frac{\partial^2}{\partial x^2}, \quad \frac{\partial^2}{\partial m'^2} = \epsilon\frac{\partial^2}{\partial y^2}. \tag{10}$$

Following the steps used by Duan for a similar model [39], we first insert Eqs. (7), (9), and (10) into Eq. (6) and expand the resulting expression up to the fourth order in powers of ϵ. Next, we set the coefficient proportional to lowest order (ϵ^2) equal to zero and obtain

$$\left(\upsilon_1^2 - \overline{u}_{01}^2\right)\frac{\partial^2\psi}{\partial x^2} + \left(\upsilon_2^2 - \overline{u}_{02}^2\right)\frac{\partial^2\psi}{\partial y^2} + 2\upsilon_1\upsilon_2\frac{\partial^2\psi}{\partial x\partial y} = 0. \tag{11}$$

By introducing the operators

$$\hat{A} = \upsilon_1\frac{\partial}{\partial x} + \upsilon_2\frac{\partial}{\partial y}, \quad \hat{B} = \overline{C}_{r1}\frac{\partial^2}{\partial x^2} + \overline{C}_{r2}\frac{\partial^2}{\partial y^2}, \tag{12}$$

the remaining expression, which consists of the terms of orders ϵ^3 and ϵ^4, may at last be written as

$$\hat{A}\left[2\frac{\partial\psi}{\partial\tau} + \hat{A}(\alpha\psi^2 - \epsilon\beta\psi^3 + \hat{B}\psi) - 2\epsilon\frac{\partial}{\partial\tau}(\alpha\psi^2 + \hat{B}\psi)\right] = 0. \tag{13}$$

From the definition of the operator $\hat{A}$ given in Eq. (12), we deduce that the expression in the square brackets in the last equation above is an arbitrary function of τ. Choosing this function as zero for simplicity, we get

$$2\frac{\partial\psi}{\partial\tau} + \hat{A}(\alpha\psi^2 - \epsilon\beta\psi^3 + \hat{B}\psi) = 2\epsilon\frac{\partial}{\partial\tau}(\alpha\psi^2 + \hat{B}\psi). \tag{14}$$

The above relation is a (2+1)-dimensional generalized modified Zakharov-Kuznetsov (GmZK) equation which comprises classical terms in its left-hand side while non-standard terms are gathered in its right-hand side. Specific cases of this equation have been found nearly in all branches of physics, especially in fluid dynamics, nonlinear lattice, plasma physics, nonlinear optics, etc. For example, when the term in the right hand side is dropped, Eq. (14) reduces to the modified Zakharov-Kuznetsov (mZK), and describes the case where the propagation occurs mainly in the longitudinal direction ($\upsilon_2 = 0$) [39–42,47,48]. Similarly, it reduces to the ZK equation [49–51] if one sets $\beta = 0$. The left-hand side of Eq. (14) can be also reduced to the modified Korteweg–de Vries (mKdV) equation investigated in Refs. [52,53] if one sets $\overline{C}_{r2} = 0$. If the cubic nonlinearity parameter $\beta = 0$ and, additionally, $\overline{C}_{r2} = 0$, Eq. (14) reduces to be the well-known KdV equation [54].

By solving Eqs. (11) and (14), we obtain the solution of Eq. (2). To this end, we define the single variable

$$z = x\cos(\theta) + y\sin(\theta) - \upsilon_c\tau, \tag{15}$$

where υ_c is the front wave velocity and θ the propagation direction of the wave. By considering this definition, Eq. (11) becomes the following ordinary differential equation:

$$\left[\left(\upsilon_1^2-\overline{u}_{01}^2\right)\cos^2(\theta)+\left(\upsilon_2^2-\overline{u}_{02}^2\right)\sin^2(\theta)+2\upsilon_1\upsilon_2\cos(\theta)\sin(\theta)\right]\frac{d^2\psi}{dz^2}=0, \tag{16}$$

from which we can express υ_1 and υ_2 as

$$\upsilon_1=\upsilon_0\cos(\theta),\quad \upsilon_2=\upsilon_0\sin(\theta) \tag{17}$$

with

$$\upsilon_0=\sqrt{\overline{u}_{01}^2\cos^2(\theta)+\overline{u}_{02}^2\sin^2(\theta)}. \tag{18}$$

From Eq. (17), we remark that the dominant propagation direction depends on the choice of the parameter θ. For instance, when $\theta\longrightarrow 0$, we have $\sin(\theta)\longrightarrow 0$, $\upsilon_2\longrightarrow 0$, $\cos(\theta)\longrightarrow 1$, and $\upsilon_1\longrightarrow\upsilon_0$. In this case, the propagation occurs dominantly in the n direction. However, if $\theta\longrightarrow\pi/2$, we have $\sin(\theta)\longrightarrow 1$, $\upsilon_2\longrightarrow\upsilon_0$, $\cos(\theta)\longrightarrow 0$, and $\upsilon_1\longrightarrow 0$. Then the dominant motion will rather be in the m direction.

By inserting Eqs. (15) and (17) into Eq. (14), we obtain after integration and setting the constant of integration to zero

$$-2\upsilon_c\psi+\upsilon_0\alpha\psi^2+\upsilon_0\overline{C}_r\frac{d^2\psi}{dz^2}+\epsilon\left(2\upsilon_c\alpha\psi^2-\upsilon_0\beta\psi^3+2\upsilon_c\overline{C}_r\frac{d^2\psi}{dz^2}\right)=0 \tag{19}$$

with $\overline{C}_r=\overline{C}_{r1}\cos^2(\theta)+\overline{C}_{r2}\sin^2(\theta)$.

B. Dynamical studies

Various solutions of Eq. (19) can be obtained depending on both the value of the parameter υ_c and the initial or boundary conditions. To present an instructive overview of these solutions, we adopt the dynamical systems technique that was pioneered in the 1990s by Flach while investigating discrete Hamiltonian lattices [55,56]. Thus, assuming that $\overline{C}_r(\upsilon_0+2\epsilon\upsilon_c)\neq 0$, we reduce Eq. (19) to a two-dimensional dynamical system

$$\begin{aligned}\frac{d\psi}{dz}&=\phi,\\ \frac{d\phi}{dz}&=\frac{\psi}{\overline{C}_r(\upsilon_0+2\epsilon\upsilon_c)}(2\upsilon_c-\alpha(\upsilon_0+2\epsilon\upsilon_c)\psi+\epsilon\upsilon_0\beta\psi^2).\end{aligned} \tag{20}$$

Obviously, system (20) has the Hamiltonian

$$H(\psi,\phi)=\phi^2-\frac{2\upsilon_c}{\overline{C}_r(\upsilon_0+2\epsilon\upsilon_c)}\psi^2+\frac{2\alpha}{3\overline{C}_r}\psi^3-\frac{\epsilon\upsilon_0\beta}{2\overline{C}_r(\upsilon_0+2\epsilon\upsilon_c)}\psi^4. \tag{21}$$

It is well-known that each of the level curves of the first integral of an ODE corresponds to a solution of the latter for some set of initial conditions. For given values of the parameters of the ODE considered, such a level curve is the solution of the equation $H(\psi,\phi)=h$; in which changing the constant h amounts to considering a different set of initial conditions.

We observe that system (20) has many fixed points or stationary states according to the sign of the quantities $\Delta_1=\alpha^2(\upsilon_0+2\epsilon\upsilon_c)^2-8\upsilon_c\epsilon\upsilon_0\beta$, υ_c, and ϵ. In fact, $O(0,0)$ is always an equilibrium point of Eq. (20) independently of the values and the sign of these parameters. When $\Delta_1>0$, system (20) has two additional equilibrium points represented by $A_\pm(\psi_{0\pm},0)$, with

$$\psi_{0\pm}=\frac{\alpha(\upsilon_0+2\epsilon\upsilon_c)\pm\sqrt{\Delta_1}}{2\epsilon\upsilon_0\beta}. \tag{22}$$

Let $M(\psi_j,\phi_j)$ be the coefficient matrix of the linearized system of Eq. (20) at an equilibrium point (ψ_j,ϕ_j) and $J(\psi_j,\phi_j)$ be its Jacobian determinant. Thus, we have

$$J_0=J(0,0)=-\frac{2\upsilon_c}{\overline{C}_r(\upsilon_0+2\epsilon\upsilon_c)}, \tag{23a}$$

$$J_+=J(\psi_+,0)=\frac{(2\alpha(\upsilon_0+2\epsilon\upsilon_c)\psi_+-3\epsilon\upsilon_0\beta\psi_+^2-2\upsilon_c)}{\overline{C}_r(\upsilon_0+2\epsilon\upsilon_c)}, \tag{23b}$$

$$J_-=J(\psi_-,0)=\frac{(2\alpha(\upsilon_0+2\epsilon\upsilon_c)\psi_--3\epsilon\upsilon_0\beta\psi_-^2-2\upsilon_c)}{\overline{C}_r(\upsilon_0+2\epsilon\upsilon_c)}. \tag{23c}$$

The theory of planar dynamical systems gives the following results for an equilibrium point of a planar integrable system [57,58]:

(i) If $J<0$, then the equilibrium point is a saddle point.

(ii) If $J>0$ and $\mathrm{Trace}(M(\psi_j,\phi_j))=0$, then it is a center point.

(iii) If $J>0$ and $(\mathrm{Trace}(M(\psi_j,\phi_j)))^2-4J(\psi_j,\phi_j)\geqslant 0$, then it is a node point.

(iv) If $J=0$ and the Poincaré index of the equilibrium point is 0, then this equilibrium point is a cusp.

By analyzing the formula (23), we easily determine the type of equilibrium point. We distinguish the following three situations. First, for $\upsilon_c>0$, $A_+(\psi_{0+},0)$ and $O(0,0)$ are saddle points and $A_-(\psi_{0-},0)$ is a center. Next, for $-\frac{\upsilon_0}{2\epsilon}<\upsilon_c<0$ the equilibrium point $O(0,0)$ is a center while the two others, $A_\pm(\psi_{0\pm},0)$, are saddle points. Finally, when $-\frac{\upsilon_0}{2\epsilon}>\upsilon_c$, there is a change in the properties of the above equilibrium points, $O(0,0)$ becomes a saddle point while $A_\pm(\psi_{0\pm},0)$ are the centers.

H being the function defined in Eq. (21) and $\psi_{0\pm}$ given by Eq. (22), we let

$$h_0=H(0,0),\quad h_+=H(\psi_{0+},0),\quad h_-=H(\psi_{0-},0). \tag{24}$$

Then we notice that for given values of the system's parameters $h_+=h_0=0$ if the front velocity υ_c takes one of the critical values

$$\upsilon_{cr\pm}=\frac{\upsilon_0}{2\epsilon}\left(\left(\frac{9\beta}{4\alpha^2}-1\right)\pm\sqrt{\left(1-\frac{9\beta}{4\alpha^2}\right)^2-1}\right). \tag{25}$$

By using the above information, we can easily do a qualitative analysis of system (20) and deduce the bifurcations of its phase portraits which is represented in Fig. 4.

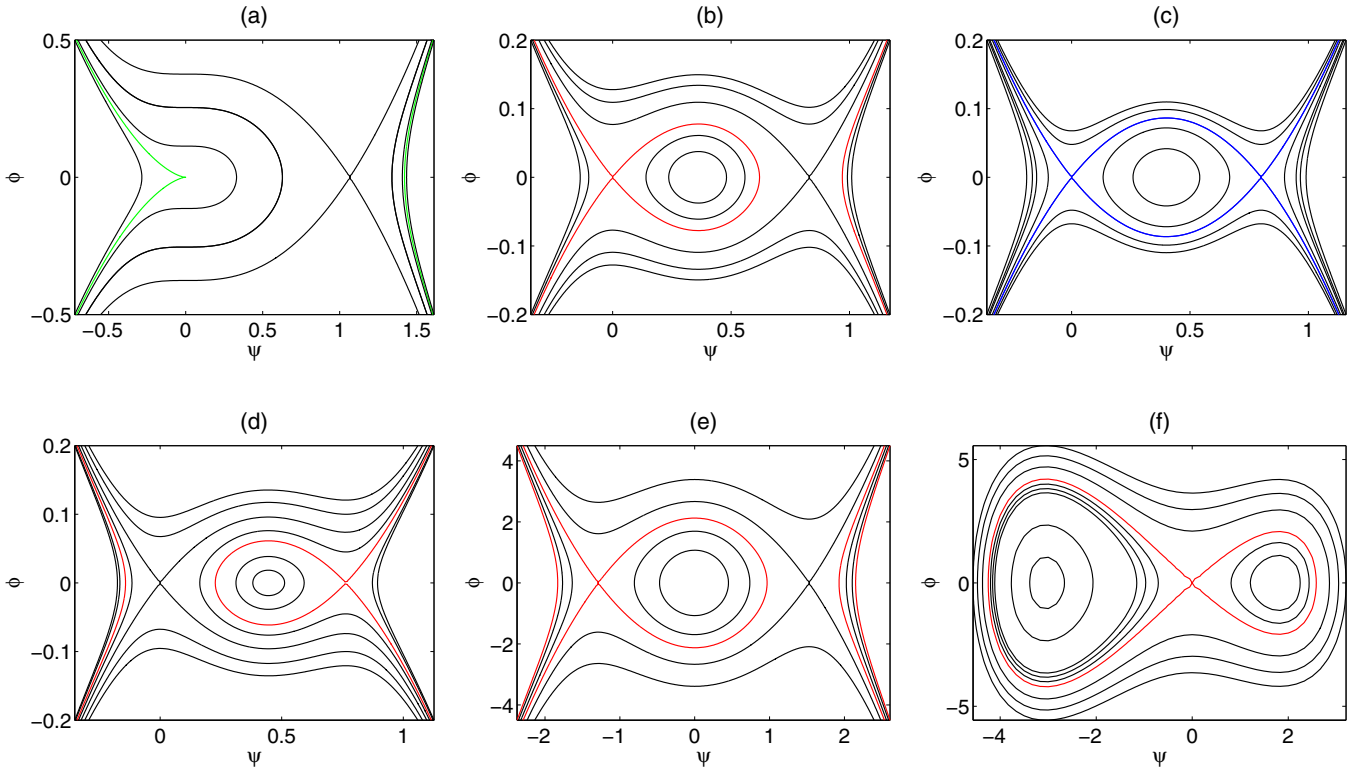

FIG. 4. Bifurcations of phase portraits of system (20) in the (ψ, ϕ)-phase plane for $\overline{u}_{01} = \overline{u}_{02} = 2.5786 \times 10^6\,\mathrm{rad}/s$, $\overline{C}_{r1} = \overline{C}_{r2} = 0.3$, $\theta = \pi/32$, $\alpha = 0.21V^{-1}$, $\beta = 0.197V^{-2}$, (a) $\upsilon_c = 0$, (b) $0 < \upsilon_c < \upsilon_{cr-}$ or $\upsilon_c > \upsilon_{cr+}$, (c) $\upsilon_c = \upsilon_{cr\pm}$, (d) $\upsilon_{cr-} < \upsilon_c < \upsilon_{cr+}$, (e) $-\upsilon_0/2\epsilon < \upsilon_c < 0$, (f) $\upsilon_c < -\upsilon_0/2\epsilon$.

These figures are obtained for the following numerical values of parameters: $\alpha = 0.21V^{-1}$, $\beta = 0.197V^{-2}$, $\overline{C}_{r1} = \overline{C}_{r2} = 0.3$, $\overline{u}_{01} = \overline{u}_{02} = 2.58 \times 10^6\,\mathrm{rad}/s$, $\theta = \pi/3$, and $\upsilon_c = 7 \times 10^5\,\mathrm{rad}/s$.

As we see in Fig. 4, the velocity υ_c plays an important role in the type of solitary wave propagating in our network. We distinguish various types of curves as follows: (a) A homoclinic orbit (red curve) corresponds to bright solitary waves (BSW), dark solitary waves (DSW) or grey solitary waves (GSW) solution of equation (23). (b) A periodic orbit (closed black curve) corresponds to a periodic traveling wave solution of Eq. (23). (c) The heteroclinic orbit (blue curve) correspond to kink and anti-kink solitary wave solutions of equation (23). (d) The black arch curve corresponds to a breaking wave solution of Eq. (23). From these figures, we summarize crucial conclusions as follows. (i) If $\upsilon_c \neq 0$, system (20) always has either an homoclinic orbit which is asymptotic to the saddle and enclosing the center, or a pair of heteroclinic orbits which connect the saddle points. There also exists in this case a family of periodic orbits which enclose the centers. (ii) When $\upsilon_c = 0$, the equilibrium point $O(0, 0)$ is a cusp.

IV. BRIGHT, DARK, KINK, AND ANTI-KINK SOLITARY WAVES

This section is devoted to the computation of the exact representations of the solitary wave solutions of Eq. (19) which correspond to bounded traveling wave solutions of Eq. (2). We restrict ourselves, for simplicity, to the case where $H(\psi, \phi) = h_0 = 0$. Thus, Eq. (21) can be written in the form

$$\phi^2 = \delta\psi^2\left(\psi^2 - \frac{4\alpha(\upsilon_0 + 2\epsilon\upsilon_c)}{3\epsilon\upsilon_0\beta}\psi + \frac{4\upsilon_c}{\epsilon\upsilon_0\beta}\right) \tag{26}$$

with

$$\delta = \frac{\epsilon\upsilon_0\beta}{2\overline{C}_r(\upsilon_0 + 2\epsilon\upsilon_c)}. \tag{27}$$

Let

$$f(\psi) = \psi^2 - \frac{4\alpha(\upsilon_0 + 2\epsilon\upsilon_c)}{3\epsilon\upsilon_0\beta}\psi + \frac{4\upsilon_c}{\epsilon\upsilon_0\beta}, \tag{28}$$

$$\Delta = \left(\frac{4\alpha(\upsilon_0 + 2\epsilon\upsilon_c)}{3\epsilon\upsilon_0\beta}\right)^2 - \left(\frac{16\upsilon_c}{\epsilon\upsilon_0\beta}\right). \tag{29}$$

If $\Delta > 0$, $f(\psi)$ admits two real roots $\psi_1 = \frac{1}{2}(\frac{4\alpha(\upsilon_0+2\epsilon\upsilon_c)}{3\epsilon\upsilon_0\beta} + \sqrt{\Delta})$ and $\psi_2 = \frac{1}{2}(\frac{4\alpha(\upsilon_0+2\epsilon\upsilon_c)}{3\epsilon\upsilon_0\beta} - \sqrt{\Delta})$. By using the first equation of the system (20) one obtains

$$z - z_0 = \int \frac{1}{\psi\sqrt{\delta(\psi - \psi_1)(\psi - \psi_2)}}\,d\phi. \tag{30}$$

The exact solutions of Eq. (19) are obtained from the results of the integral in Eq. (30). The kind of these results depends both on the relative magnitudes of the system's parameters and on the value of the velocity υ_c as discussed below.

A. Bright solitary wave [Figs. 4(b) and 4(f)]

In this subsection, we focus our attention on the derivation of bright solitary wave solutions of GmZK equation obtained above. This type of solution exists when $\upsilon_c > 0$ and $\upsilon_c \neq \upsilon_{cr}$.

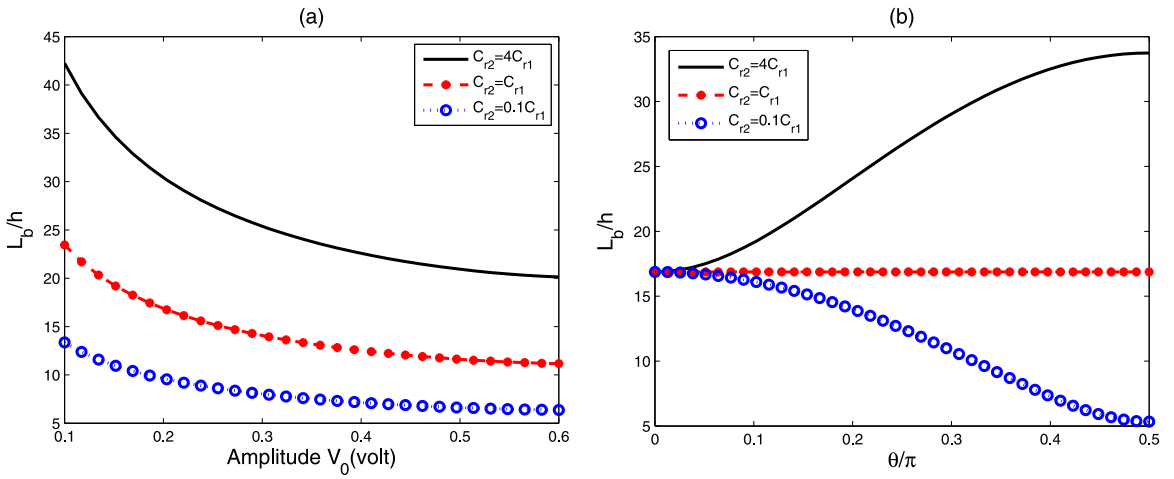

FIG. 5. Variation of bright pulse width L_b for $\overline{u}_{01} = \overline{u}_{02} = 2.5786 \times 10^6$ rad/s, $\overline{C}_{r1} = 0.3$, $\alpha = 0.21V^{-1}$, $\beta = 0.197V^{-2}$: (a) as a function of wave amplitude V_0: $\theta = \pi/3$, $\overline{C}_{r2} = 4\overline{C}_{r1}$, $\overline{C}_{r1}$, and $0.1\overline{C}_{r1}$. (b) as a function of the propagation direction θ: $V_0 = 0.2$, $\overline{C}_{r2} = 4\overline{C}_{r1}$, $\overline{C}_{r1}$, and $0.1\overline{C}_{r1}$.

It corresponds to the curves defined by $H(\psi, \phi) = 0$ and has the following parametric representation:

$$\psi(z) = \frac{6\upsilon_c}{\alpha(\upsilon_0 + 2\epsilon\upsilon_c)} \frac{1}{1 + b_0 \cosh(\mu z)}, \tag{31}$$

where

$$b_0 = \frac{1}{2\alpha}\sqrt{4\alpha^2 - \frac{36\beta\epsilon\upsilon_c\upsilon_0}{(\upsilon_0 + 2\epsilon\upsilon_c)^2}}, \quad \mu = \sqrt{\frac{4\upsilon_c\delta}{\beta\epsilon\upsilon_0}}. \tag{32}$$

According to Eq. (7), we find the following two-dimensional pulse-like signal voltage for the network:

$$V_{n,m}(t) = \frac{V_0}{1 + \gamma_0 \cosh[\mu_c(\xi - \upsilon_p t)]} \tag{33}$$

with

$$\xi = \frac{s}{\lambda}((n - n_0)\cos(\theta) + (m - m_0)\sin(\theta)),$$
$$\upsilon_p = \upsilon_0\left(1 + \frac{\alpha V_0}{6 - 2\alpha V_0}\right), \quad \mu_c = \sqrt{\frac{\alpha V_0}{3\overline{C}_r}},$$
$$\gamma_0 = \sqrt{1 - \frac{\beta V_0(3 - \alpha V_0)}{2\alpha}}, \quad V_0 \neq \frac{3}{\alpha}; \tag{34}$$

υ_0 and $\overline{C}_r$ being defined by Eqs. (17) and (19), respectively.

By using Eq. (33), one determines that the soliton width L_b is given by

$$L_b = \frac{2\lambda}{\mu_c s}\cosh^{-1}\left(\frac{1 + 2\gamma_0}{\gamma_0}\right). \tag{35}$$

Equation (35) shows clearly that the analytical expression of the bright soliton pulse width depends on the pulse amplitude through γ_0. It is the most crucial property of the bright pulse

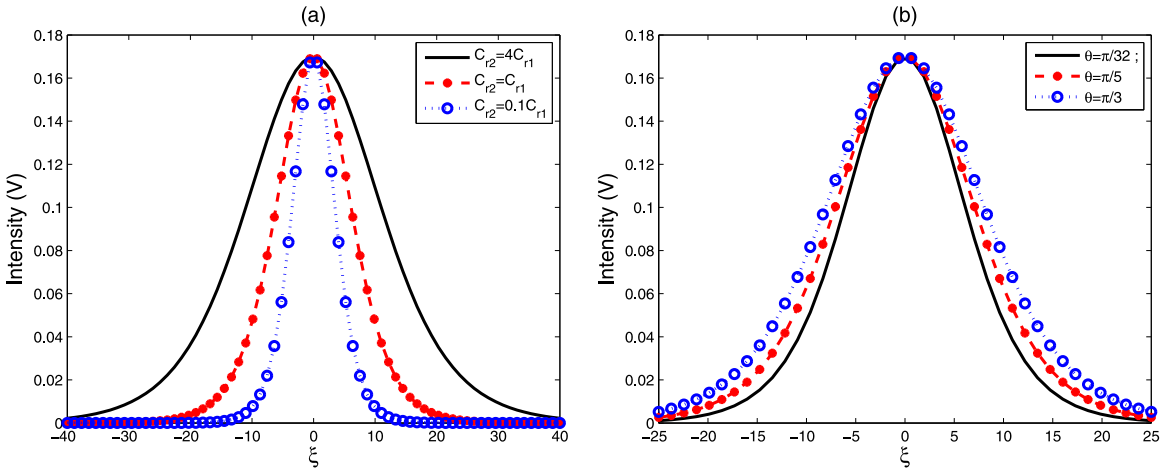

FIG. 6. Shape of the bright soliton (33) at $t = 0$ for $\overline{u}_{01} = \overline{u}_{02} = 2.5786 \times 10^6$ rad/s, $\overline{C}_{r1} = 0.3$, $\alpha = 0.21V^{-1}$, $\beta = 0.197V^{-2}$, $V_0 = 0.3$: (a) $\theta = \pi/3$ and for different values the reduced coupling capacitance $\overline{C}_{r2}$. (b) $\overline{C}_{r2} = 2\overline{C}_{r1}$ and for different values the propagation direction θ.

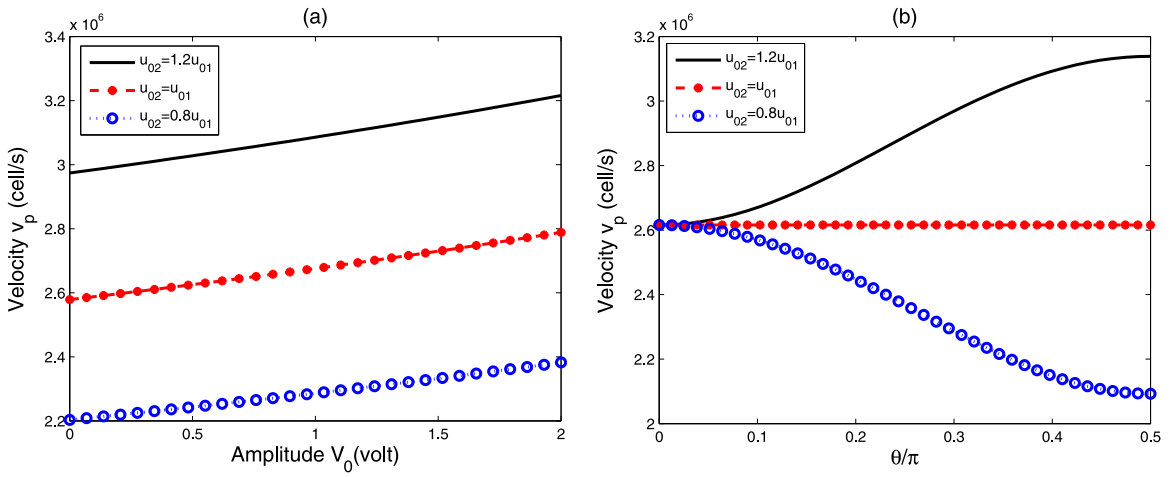

FIG. 7. Variation of envelope velocity υ_p for $\overline{u}_{01} = 2.5786 \times 10^6\,\mathrm{rad}/s$, $\overline{C}_{r1} = \overline{C}_{r2} = 0.3$, $\alpha = 0.21V^{-1}$, $\beta = 0.197V^{-2}$: (a) as a function of amplitude wave V_0; $\theta = \pi/3$ and $\overline{u}_{02} = 1.2\overline{u}_{01}$, $\overline{u}_{01}$, and $0.8\overline{u}_{01}$. (b) As a function of the propagation direction θ: $V_0 = 0.2$, $\overline{u}_{02} = 1.2\overline{u}_{01}$, $\overline{u}_{01}$, and $0.8\overline{u}_{01}$.

and contrasts with the expression of the compact pulse width which is independent of the pulse amplitude [34,59]. Let us note here that the pulse is described by four main parameters: the width, the speed, the amplitude and the parameter γ_0 which is a function of the quadratic and cubic nonlinearity parameters α and β.

Figure 5 shows some representations of this width and it appears obviously that an increase in the reduced coupling capacitance constant $\overline{C}_{r2}$ results in an increase of this width. Figure 5(a) shows that the width decreases when the pulse amplitude increases. Similarly, the effects of the reduced propagation direction θ are more clearly seen in Fig. 5(b). It is obvious that when $\overline{C}_{r1} = \overline{C}_{r2}$, the pulse width is independent on the reduced propagation direction. It also shows that the intensity width is an increasing or a decreasing function of the reduced propagation direction depending on whether $\overline{C}_{r2} > \overline{C}_{r1}$ or $\overline{C}_{r2} < \overline{C}_{r1}$, respectively. These results suggest to study the evolution of the pulse shape for different values $\overline{C}_{r2}$ and θ. Our investigations lead to the plots of Fig. 6 which establish that the shape of the pulse changes with $\overline{C}_{r2}$ and θ. Thus, the parameters $\overline{C}_{r2}$ and θ can be used to control the shape of the bright solitary wave solution. We can also observe from Figs. 5 that the width L_b is always greater than one. In fact, it is seen that it can even be sufficiently larger, which then justifies the use of the continuum limit approximation.

From Eq. (34), we can see that the envelope velocity of pulse is nonlinearly dependent on the amplitude V_0 of the signal. The existence of the soliton solution (33) is subjected to the constraint: $3 - \alpha V_0 > 0$. Thus, the envelope velocity increases with the amplitude V_0. These results are more clearly seen in Fig. 7(a) for different values of the coupling characteristic frequencies $\overline{u}_{02}$ of the network. Similarly, Fig. 7(b) shows the effects of the reduced propagation direction θ on this velocity. It is obvious that for $\overline{u}_{01} = \overline{u}_{02}$, the velocity of the pulse is independent on the reduced propagation direction. It also shows that the magnitude of velocity is an increasing function of the reduced propagation direction for $\overline{u}_{01} < \overline{u}_{02}$ while for $\overline{u}_{01} > \overline{u}_{02}$, it becomes a decreasing function of the same.

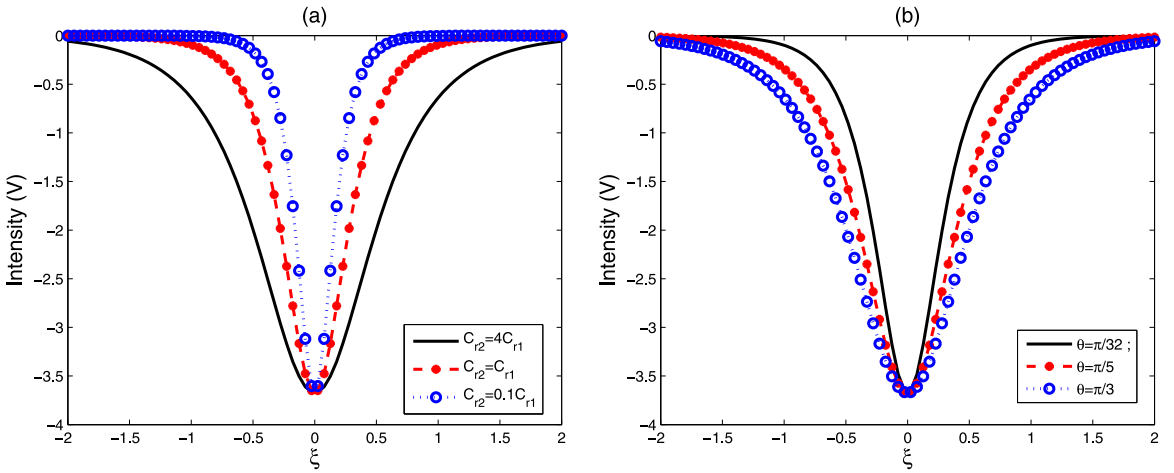

FIG. 8. Shape of the dark soliton (36) at $t = 0$ for $\overline{u}_{01} = \overline{u}_{02} = 2.5786 \times 10^6\,\mathrm{rad}/s$, $\overline{C}_{r1} = 0.3$, $\alpha = 0.21V^{-1}$, $\beta = 0.197V^{-2}$, $V_0 = 0.3$: (a) $\theta = \pi/3$ and for different values the reduced coupling capacitance $\overline{C}_{r2}$. (b) $\overline{C}_{r2} = 4\overline{C}_{r1}$ and for different values the reduced propagation direction θ.

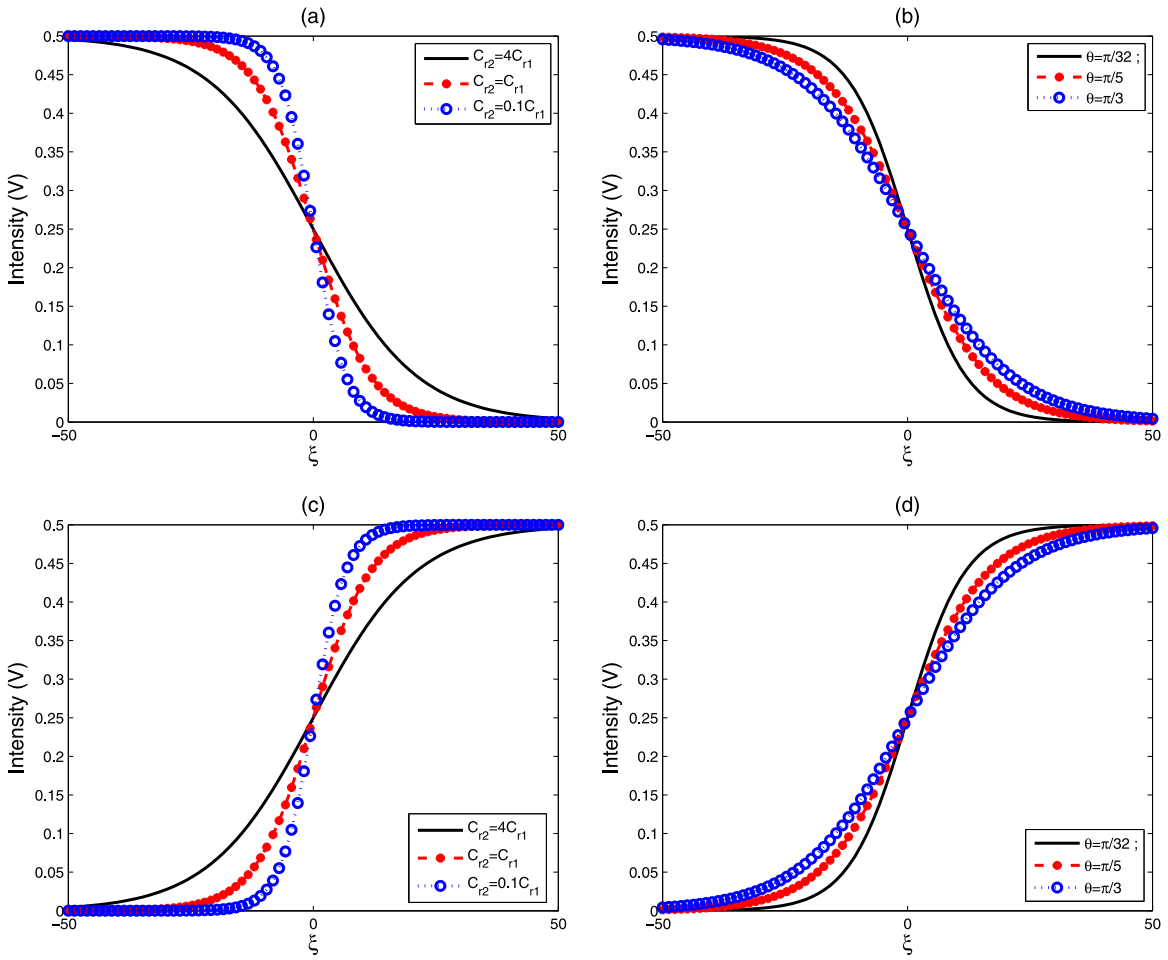

FIG. 9. Shape of the antikink (first row) and kink (second row) soliton (40) at $t = 0$ for $\overline{C}_{r1} = 0.3, \alpha = 0.21V^{-1}, \beta = 0.197V^{-2}, V_0 = 0.5$: (a) and (c) $\theta = \pi/3$ and for different values the reduced transverse capacitance $\overline{C}_{r2}$. (b) and (d) $\overline{C}_{r2} = 4\overline{C}_{r1}$ and for different values the propagation direction θ.

B. Dark solitary wave [Fig. 4(f)]

When $\upsilon_c < -\upsilon_0/(2\epsilon)$, the GmZK equation admits dark and bright solitary wave as solutions; they correspond to the pair of homoclinic orbits of Fig. 4(f). The right homoclinic orbit has the same parametric representation as Eq. (33) while the left homoclinic orbit has the following parametric representation:

$$V_{n,m}(t) = \frac{V_0}{1 - \gamma_0 \cosh[\mu_c(\xi - \upsilon_p t)]}. \tag{36}$$

It is equally characterized by its amplitude V_0, the speed υ_p, the parameter γ_0, and the width

$$L_d = \frac{2\lambda}{\mu_c s} \cosh^{-1}\left(\frac{2\gamma_0 - 1}{\gamma_0}\right). \tag{37}$$

The solution (36) represents a dark solitary wave of Eq. (2), where γ_0 is characteristic depth parameter that depends on the relative wave amplitude V_0 and network parameters, namely, the coefficients α and β of the quadratic and cubic terms, respectively. If $0 < \gamma_0 \leqslant 1$, this solution is not physically relevant. Hence, $\gamma_0 > 1$ is the necessary condition for the system to exhibit this solution. When $\beta = 0$, we have $\gamma_0 = 1$ and solution (36) does not exist. Thus, the existence of this dark pulse soliton is subjected to the presence of the cubic nonlinearity β within Eq. (1).

The parameters of this dark soliton including its speed υ_p and width L_d are also dependent on the reduced propagation direction θ, coupling characteristic frequencies $\overline{u}_{02}$, and reduced coupling capacitance $\overline{C}_{r2}$. The effect of the variations of these parameters with $\overline{C}_{r2}$ and θ are similar to the case of bright soliton (Figs. 5 and 7). These results are confirmed by Fig. 8, where the shape of the dark soliton (36) are portrayed for different values of reduced coupling capacitance constant $\overline{C}_{r2}$ and reduced propagation direction θ.

C. Kink and anti-kink solitary waves [Fig. 4(c)]

As shown above by the dynamical studies, the kind of the solitary wave which can propagate in the network strongly depends on the magnitude of the front wave velocity. Here, we find the exact profile of kink and anti-kink solitary waves solution of differential equations (2) governing the dynamics of signals in our coupled Noguchi nonlinear electrical transmission line. This solitary wave exists if $\upsilon_c = \upsilon_{cr\pm}$ [see Fig. 4(c)]. In this case, we have $\Delta = 0$ and we see from $H(\psi_+, 0) =$

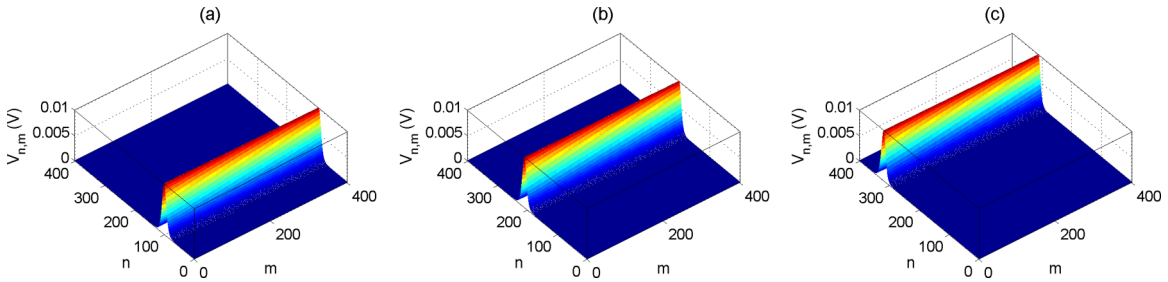

FIG. 10. Bright signal voltage (in volts) as a function of the propagating direction n and transverse direction m of the network at given times of the propagation of wave with characteristic parameter $\theta = \pi/64$, $V_0 = 0.02$, $\mu_c = 0.2160$, $\upsilon_p/u_0 = 1.0007$, and $\gamma_0 = 0.9858$. (a) The initial signal voltage is the bright pulse solitary wave located at cell $(n_0, m_0) = (100, 100)$. (b) and (c) show the wave at given times (in units of u_0) of propagation: $t_1 = 110$ and $t_2 = 220$, respectively. The wave experiences are uniform, and the propagation is stable along the network.

$h_+ = 0$ that corresponding to the two heteroclinic orbits,

$$\phi^2 = \delta\psi^2(\psi_0 - \psi)^2, \quad \text{with} \quad \psi_0 = \frac{2\alpha(\upsilon_0 + 2\epsilon\upsilon_c)}{3\epsilon\upsilon_0\beta}. \quad (38)$$

Thus, we obtain

$$\psi(z) = \frac{\psi_0}{1 + \exp\left(\pm\frac{\psi_0}{2}\sqrt{\delta}z\right)}. \quad (39)$$

According to Eq. (7), we find the following two-dimensional kink and antikink-like voltage signal for the network:

$$V_{n,m}(t) = \frac{V_0}{1 + \exp[\pm\mu_k(\xi - \upsilon_k t)]} \quad (40)$$

with

$$\xi = \frac{s}{\lambda}((n - n_0)\cos(\theta) + (m - m_0)\sin(\theta)),$$
$$\upsilon_k = \frac{\upsilon_0}{2}\left(\left(\frac{9\beta}{4\alpha^2} + 1\right) \pm \sqrt{\left(1 - \frac{9\beta}{4\alpha^2}\right)^2 - 1}\right), \quad (41)$$
$$\mu_k = \frac{1}{2}\sqrt{\frac{\alpha V_0}{3\overline{C}_r}};$$

υ_0 and $\overline{C}_r$ being defined by Eqs. (17) and (19), respectively. Equation (40) represents the kink-soliton solution and antikink-soliton solution of a coupled Noguchi nonlinear electrical transmission line. It should be noted that, here, the characteristic parameters $L_k = 1/\mu_k$ and υ_k can be written as $L_k = K_1 L_b$ and $\upsilon_k = K_2\upsilon_p$, where K_1 and K_2 are positive constants and υ_p and L_b given respectively by Eqs. (34) and (35). Consequently, they have similar representations to those of Figs. 5 and 7 for different values of the coupling network parameters $\overline{C}_{r2}$ and $\overline{u}_{02}$. Thus, it is obvious that an increase in the degree of reduced coupling capacitance $\overline{C}_{r2}$ results in an increase of the kink and anti-kink solitary width. This effect is more clearly seen in Fig. 9 where the shape of kink soliton and anti-kink soliton solutions (40) are plotted. It should be noted that, as in case of pulse soliton, the width of kink soliton increase with $\overline{C}_{r2}$.

Before ending the section, it is important to make some remarks resulting from the above investigations. The coupling elements play a very significant role in this model of coupled Noguchi network and can be used to control the various parameters of solitary wave which is propagated there. For example, the width of solitary wave can be controlled by the reduced coupling capacity $\overline{C}_{r2}$. In the same way, the front wave velocity can be modified while exploiting the coupling characteristic frequency $\overline{u}_{02}$.

V. NUMERICAL INVESTIGATIONS

In the preceding section, we have investigated the transverse solitary wave solution in a nonlinear electrical transmission line governed by a nonlinear differential equation. The influence of the speed parameter υ_c was mainly examined

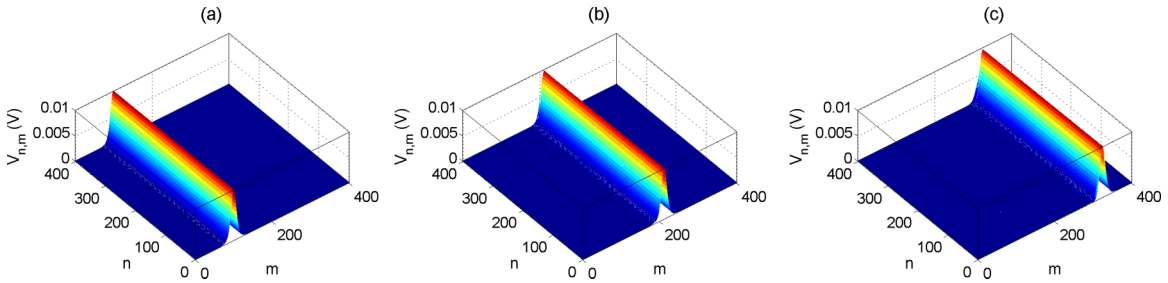

FIG. 11. Bright signal voltage (in volts) as a function of the propagating direction m and longitudinal direction n of the network at given times of the propagation of wave with characteristic parameter $\theta = 100\pi/202$, $V_0 = 0.02$, $\mu_c = 0.2160$, $\upsilon_p/u_0 = 1.0007$, and $\gamma_0 = 0.9858$. (a) The initial signal voltage is the bright pulse solitary wave located at cell $(n_0, m_0) = (100, 100)$. (b) and (c) show the wave at given times (in units of u_0) of propagation: $t_1 = 110$ and $t_2 = 220$, respectively. The wave experiences are uniform, and the propagation is stable along the network.

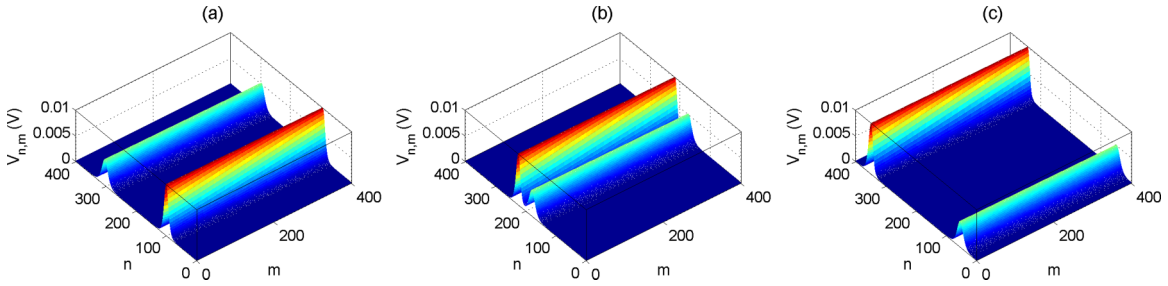

FIG. 12. Elastic collision of two bright signal voltage (33) as a function of the propagating direction n and transverse direction m of the network at given times of the propagation of wave. (a) At $t = 0$, the first located at cell $(n_0, m_0) = (100, 100)$ with $\theta = \pi/64$, $V_0 = 0.02$, $\mu_c = 0.2160$, $\upsilon_p/u_0 = 1.0007$, and $\gamma_0 = 0.9858$. Second located at cell $(n_0, m_0) = (300, 300)$ with $V_0 = 0.01$, $\mu_c = 0.1528$, $\upsilon_p/u_0 = -1.0004$, and $\gamma_0 = 0.9929$. (b) and (c) show the wave at given times (in units of u_0) of propagation: $t_1 = 125$ and $t_2 = 250$, respectively. The wave experiences are uniform, and remained coherent after collision along the network.

and the results are obtained. In this section, we report the results of the numerical experiments that we have performed on the exact discrete equation (2) of the network, using the fourth-order Runge Kutta method with normalized integration time step $h_0 = \upsilon_0 \Delta t = 10^{-2}$ in order to check the theoretical predictions. Let us consider the following characteristic network parameters: $L_1 = L_2 = 0.47mH$ and $C_1 = C_2 = 96pF$ for linear inductance and capacitor, respectively, in the n and m directions. Also, the nonlinear capacitor in the shunt branch is the well-known BB112 nonlinear diode with the characteristics: $C_0 = 32pF$, $\alpha = 0.21V^{-1}$, and $\beta = 0.197V^{-2}$. As initial condition, we introduce one of the above solitary wave signal; for some chosen value of the amplitude parameter V_0. It is important to note that this choice is not completely arbitrary as the value should not lead to the violation of any of the specific conditions under which the solitary wave considered has been derived. It appears for instance that, for dark solitary wave, the small amplitude assumption which amounts to $V_0/(\gamma_0 - 1) \ll 1$ on account of the other constraint $1 < \gamma_0$ noted earlier in Sec. IV B, is fulfilled for no value of V_0. This indicates that not all of the solitary waves predicted by the analytical developments do effectively exist for concrete electrical networks. Likewise, the coexistence of different types of them, such as seen in Fig. 4(f), is not effective for the present set of network parameters' values. Then, we concentrate below on the study of bright solitons whose existence conditions are easily satisfied. The numbers of cells are taken equal to $N = M = 400$ in the propagation and transverse directions. The ratio of the cell size to the wavelength is taken as $s/\lambda = 0.1$. For the effectiveness of these simulations, we consider the case of positive front wave velocity υ_c to examine the behavior of the solitary wave during its progression in the system.

Thus, we present in Figs. 10 and 11 the evolution of bright solitary wave (33). The reduced propagation direction of solitary wave is $\theta = \pi/64$ for Fig. 10 and $\theta = 100\pi/202$ for Fig. 11. We observe from these figures that the initial electrical signal voltage propagates with constant amplitude, without distortion of shape, and with constant reduced velocity $\upsilon_p/\upsilon_0 = 1.0071$, which is in full agreement with the theoretical prediction.

Since the wave velocity υ_0 is amplitude dependent, two adjacent pulse soliton will interact in the network because they propagate at the different speed. Thus, the interactions of two bright pulse voltages (33) propagating in opposite directions and with different amplitudes $V_0 = 0.1$ and $V_0 = 0.05$ are depicted in Fig. 12 for $\theta = \pi/64$. It is obvious that, these bright solitons remain coherent after collision.

VI. CONCLUSION

In this paper, we have investigated both analytically and numerically the dynamics of solitary waves in a model of nonlinear electrical transmission line. This model is a two-dimensional electrical network which consists of a number of identical cells LC.

We have been particularly interested by the dynamics of the solitary waves. The differential equations governing the propagation of the signal voltage in the network has been obtained. Using the continuum limit approximations, we have first shown that the dynamics of small amplitude signals in the network can be described by a generalized modified Zakharov-Kuznetsov equation. Next, the dynamical studies of this GmZK have been carried out. We have noticed that the values of wave speed influence considerably the type of the solitary waves in the system. From these results, one can finally obtain the various two-dimensional solitary voltage signal that can be transmitted throughout the network. Direct numerical simulations on the exact equations of the network have been performed and the results have been seen to compare qualitatively very well with the theoretical predictions. In fact, we note that the wave experiences a uniform and stable propagation along the network. In the same way, these pulses keep their identities upon interacting with one another.

These interesting obtained results and the connection between the homoclinic (heteroclinic) orbits of the phase portraits and the existence of pulse (kink and anti-kink) waves could be of great use in applications such as communication and frequency modulation. Another interesting aspect of this work is that it shows the influence of the coupling elements on the angular frequency and the important role of the front wave velocity on the existence of different solitary solutions. The capacitive coupling can also be used to control the shape of these solitary wave solutions.

[1] E. Fermi, J. Pasta, and S. Ulam, in *Nonlinear Wave Motion*, Lectures in Applied Mathematics Vol. 15, edited by A. C. Newell (American Mathematical Society, Providence, 1974).

[2] N. J. Zabusky and M. D. Kruskal, Phys. Rev. Lett. **15**, 240 (1965).

[3] E. Lorin, M. Lytova, A. Memarian, and A. D. Bandrauk, J. Phys. A: Math. Theor. **48**, 105201 (2015).

[4] F. Maucher, D. Buccoliero, S. Skupin, M. Grech, A. S. Desyatnikov, and W. Krolikowski, Opt. Quantum Electron. **41**, 337 (2009).

[5] A. B. Aceves, G. Fibich, and B. Ilan, Physica D: Nonlinear Phenomena **189**, 277 (2004).

[6] M. Alidou, A. Kenfack-Jiotsa, and T. C. Kofane, Chaos, Solitons Fractals **27**, 914 (2006).

[7] R. Nath, P. Pedri, and L. Santos, Phys. Rev. Lett. **101**, 210402 (2008).

[8] C. J. McKinstrie and R. Bingham, Phys. Fluids B: Plasma Phys. **1**, 230 (1989).

[9] P. B. Ndjoko, J. M. Bilbault, S. Binczak, and T. C. Kofane, Phys. Rev. E **85**, 011916 (2012).

[10] M. Remoissenet, *Waves Called Solitons*, 3rd ed. (Springer, Berlin, 1999).

[11] A. Noguchi, Electron. Commun. Jpn. **57**, 9 (1974).

[12] Y. H. Ichikawa, T. Mitsuhaski, and K. Konno, J. Phys. Soc. Jpn **41**, 1382 (1976).

[13] T. Yoshinaga and T. Kakutani, J. Phys. Soc. Jpn. **53**, 85 (1984).

[14] F. B. Pelap and M. M. Faye, Nonlinear Oscillations **8**, 513 (2005).

[15] F. B. Pelap, J. H. Kamga, S. B. Yamgoue, S. M. Ngounou, and J. E. Ndecfo, Phys. Rev. E **91**, 022925 (2015).

[16] E. Kengne, A. Lakhssassi, and W. M. Liu, Phys. Rev. E **96**, 022221 (2017).

[17] E. Kengne and W. M. Liu, Phys. Rev. E **97**, 052205 (2018).

[18] F. B. Pelap, T. C. Kofané, N. Flytzanis, and M. Remoissenet, J. Phys. Soc. Jpn. **70**, 2568 (2001).

[19] F. B. Pelap and M. M. Faye, J. Math. Phys. **46**, 033502 (2005).

[20] E. Kengne and W. M. Liu, Phys. Rev. E **73**, 026603 (2006).

[21] D. Yemélé, P. Marquié, and J. M. Bilbault, Phys. Rev. E **68**, 016605 (2003).

[22] F. B. Pelap and M. M. Faye, J. Phys. Soc. Jpn. **76**, 074602 (2007).

[23] S. B. Yamgoué and F. B. Pelap, Phys. Lett. A **380**, 2017 (2016).

[24] I. A. Butt and J. A. D. Wattis, J. Phys. A: Math. Gen. **39**, 4955 (2006).

[25] Naranmandula and K. X. Wang, Phys. Lett. A **336**, 112 (2005).

[26] H. Buttner and H. Bilz, in *Solitons and Condensed Matter Physics*, edited by A. R. Bishop, and T. Schneider (Springer, Berlin, 1978).

[27] S. Pnevmatikos, N. Flytzanis, and M. Remoissenet, Phys. Rev. B **33**, 2308 (1986).

[28] F. B. Pelap, I. Tatsinkou, and A. Fomethe, Phys. Scr. **83**, 045009 (2011).

[29] L. Q. English, F. Palmero, J. F. Stormes, J. Cuevas, R. Carretero-González, and P. G. Kevrekidis, Phys. Rev. E **88**, 022912 (2013).

[30] E. Tala-Tebue and A. Kenfack-Jiotsa, J. Mod. Phys. **4**, 7467 (2013).

[31] E. Kengne, S. T. Chui, and W. M. Liu, Phys. Rev. E **74**, 036614 (2006).

[32] E. Kengne, V. Bozic, M. Viana, and R. Vaillancourt, Phys. Rev. E **78**, 026603 (2008).

[33] J. K. Duan and Y. L. Bai, Indian J. Phys. **92**, 369 (2018).

[34] F. Kenmogne, D. Yemélé, J. Kengne, and D. Ndjanfang, Phys. Rev. E **90**, 052921 (2014).

[35] J. Manafian and M. Lakestani, Eur. Phys. J. Plus **133**, 119 (2018).

[36] M.-m. Lin and W.-s. Duan, Chaos, Solitons Fractals **24**, 191 (2005).

[37] D. Wen-Shan, H. Xue-Ren, S. Yu-Ren, L. Ke-Pu, and S. Jian-An, Chin. Phys. Lett. **19**, 1231 (2002).

[38] E. Tala-Tebue, D. C. Tsobgni-Fozap, A. Kenfack-Jiotsa, and T. C. Kofane, Eur. Phys. J. Plus **129**, 136 (2014).

[39] W. S. Duan, Europhys. Lett **66**, 192197 (2004).

[40] J. Yu, W. J. Zhang, and X. M. Gao, Chaos, Solitons Fractals **33**, 1307 (2007).

[41] H. L. Zhen, B. Tian, H. Zhong, and Y. Jiang, Comput. Math. Appl. **68**, 579 (2014).

[42] A. Sardar, S. M. Husnine, S. T. R. Rizvi, M. Younis, and K. Ali, Nonlinear Dyn **82**, 1317 (2015).

[43] S. Abdoulkary, A. Mohamadou, and T. Beda, Commun Nonlinear Sci Numer Simulat **16**, 3525 (2001).

[44] P. Marquié, J. M. Bilbault, and M. Remoissenet, Phys. Rev. E **49**, 828 (1994).

[45] S. D. Yamigno, J. Mod. Phys. **5**, 394 (2014).

[46] B. Z. Essimbi and D. Jager, Phys. Scr. **81**, 035801 (2010).

[47] S. K. El-Labany, W. F. El-Taibany, E. E. Behery, and N. A. Zedan, Eur. Phys. J. Plus **130**, 250 (2015).

[48] H. W. Yang, Z. H. Xu, D. Z. Yang, X. R. Feng, B. S. Yin, and H. H. Dong, Adv. Diff. Eqs. **2016**, 167 (2016).

[49] E. V. Krishnan and A. Biswas, Phys. Wave Phenomena **18**, 256 (2010).

[50] G. C. Das, J. Sarma, Y.-T. Gao, and C. Uberoi, Phys. Plasmas **7**, 2374 (2000).

[51] Z. Z. Dong, Y. Chen, and Y. H. Lang, Chin. Phys. B **19**, 090205 (2010).

[52] A. Nakamura and R. Hirota, J. Phys. Soc. Jpn. **48**, 1755 (1980).

[53] S. Watanabe, J. Phys. Soc. Jpn. **53**, 950 (1984).

[54] M. Wadati, J. Phys. Soc. Jpn. **38**, 673 (1975).

[55] S. Flach, Phys. Rev. E **50**, 3134 (1994).

[56] S. Flach, Phys. Rev. E **51**, 1503 (1995).

[57] J. Li, X. Zhao, and G. Chen, Int. J. Bifurcation Chaos **19**, 1289 (2009).

[58] A. Saha, Commun. Nonlinear Sci. Numer. Simulat. **17**, 3539 (2012).

[59] C. Pokam-Nguewawea, D. Yemélé, H. Y. Donkeng, and T. C. Kofane, Commun. Nonlinear Sci. Numer. Simulat. **43**, 50 (2017).